Nucleation of an Oil Phase in a Nonionic Microemulsion-Containing Chlorinated Oil upon Systematic Temperature Quench

G. Roshan Deen*,† and Jan Skov Pedersen‡

Soft Materials Laboratory, Natural Science and Science Education, National Institute of Education, Nanyang Technological University, 1-Nanyang Walk, Singapore 637616, and Department of Chemistry and Interdisciplinary Nanoscience Center (iNANO), Aarhus University, Langelandsgade 140, Aarhus C 8000, Denmark

Received: March 15, 2010; Revised Manuscript Received: May 4, 2010

A clear and stable nonionic model microemulsion consisting of pentaoxyethylene glycol dodecyl ether ($C_{12}E_5$), water, and 1-chlorotetradecane (CLTD) was prepared. This system was subjected to a systematic temperature quench (perturbation out of equilibrium) in steps of 1.0 °C from 20.4 to 15.3 °C in the unstable region of its phase diagram. The change in turbidity (for droplet volume fractions of 0.02 and 0.08) and hydrodynamic radius (R_h) (for a droplet volume fraction of 0.02) of the system on its way to its new equilibrium was measured at each quench temperature. For small systematic temperature quenches just below the emulsification failure boundary (EFB) the turbidity decreases and remains constant indicating quick changes in the microstructures. Further lowering of temperature brings the system to the unstable region where the turbidity and light scattering increase sharply as function of time because of expulsion of excess oil from the microemulsion droplets. The newly formed oil-rich droplets grow in size as a function of time. These observations indicate the existence of a narrow but observable metastable region en route to the new equilibrium where both microemulsion droplets and larger oil-rich droplets coexist. The region in which microemulsion droplets are metastable is very narrow and is concentration-dependent. The presence of a metastable region is as for other similar systems attributed to the presence of a free energy barrier for the formation of the larger oil-rich droplets associated with curvature free energy of the surfactant film. The turbidity−time curves were converted to the radius−time curves using a model assuming monodisperse spherical droplets. The obtained results are in good agreement with the results for the hydrodynamic radius. The observed average radius from both type of measurements decreases in the metastable region. By performing calculation of the influence of eccentricity and size polydispersity on the observed radius, we have shown that the distribution of the microemulsion droplets becomes more homogeneous in the metastable region.

Introduction

Microemulsions are multicomponent systems consisting mainly of surfactant, water, and oil. These are thermodynamically stable and isotropically clear solutions consisting of microstructures that vary between 1 and 100 nm in length scale.[1−4] Depending on the type of surfactants used in the formulation of microemulsions, they can be classified as ionic and nonionic microemulsions. These systems have gained immense importance in potential applications such as in catalytic reactions, synthesis of monodisperse nanoparticles, enhanced oil recovery, preconcentrated drug formulations, and so on.[5−8] The different types of microemulsions are described by Winsor phases[7] such as oil-in-water phase (Winsor I), water-in-oil phase (Winsor II), bicontinuous phase (Winsor III), and single phase (Winsor IV). The surfactant present in the microemulsion plays a vital role in solubilizing the immiscible components viz. oil and water by reducing the surface tension at the oil−water interface. The surfactants can be classified as cationic, anionic, zwitterionic, or nonionic depending on the charge of their headgroup.[8]

Microemulsions consisting of nonionic surfactants such as alkyl poly(ethylene glycol) ether surfactants CH_3-$(CH_2)_{j-1}$-$(OCH_2CH_2)_i$−OH (C_iE_j) and *n*-alkanes have been studied in detail (with emphasis on phase behavior and microstructure), owing to the rich temperature-dependent phase behavior that is exhibited by these systems.[9−20] Here *j* represents the number of carbon atoms in the alkyl chain and *i* represent the number of ethylene oxide units of the surfactant. In these nonionic microemulsions, the formation of various microemulsion phases can be easily induced by varying the temperature of the system, which modifies the spontaneous curvature of the surfactant film.[1,2] These changes arise because of the strong temperature-dependent interactions between the ethylene oxide groups of the surfactant and water.[1] Therefore, water changes from being a good solvent at lower temperature to a poor solvent at higher temperature for this type of surfactant, thereby inducing curvature changes of the surfactant film.[12−14] This temperature-dependent curvature property at the phase inversion or balance temperature, T_0, can be quantitatively described in terms of spontaneous mean curvature of the surfactant film, H_0, as[1]

$$H_0(T) = c(T_0 - T) \quad (1)$$

where *c* is the coefficient that is dependent on the nature of the surfactant, which is $\sim 10^{-3}$ (K nm)$^{-1}$ for $C_{12}E_5$ surfactant.[15,21]

* To whom correspondence should be addressed. E-mail: roshan.gulam@nie.edu.sg.
† Nanyang Technological University.
‡ Aarhus University.

10.1021/jp102365j
Published on Web 05/21/2010

From this, it can be realized that the temperature-dependent property of C_iE_j-type surfactants forms the fundamental basis for describing the various equilibrium phases of nonionic microemulsions including emulsification.[1,2,22,23]

The phase diagram of C_iE_j microemulsions has a region with globular oil-swollen micelles, which are also called droplets. When the temperature is lowered below this droplet L_1 phase, the droplets can no longer contain all of the oil, and emulsification failure is said to be initiated. To optimize the curvature free energy of the microemulsion droplet, the spontaneous radius of the droplet, which is given by $R_0 = 1/H_0$ decreases. As a result of this, the droplets expel the oil that it holds in excess and attain a new optimal radius. Because of this perturbation in equilibrium, a new state is reached in which the droplet phase and the excess oil phase are in equilibrium, and this state is denoted as the $L_1 + O$ phase. Although this type of emulsification failure is an unwanted process in industrial applications, it can still be turned advantageous in the process of producing monodisperse latex particles,[24] gel emulsions,[25,26] and so on. Upon systematically lowering the temperature to the $L_1 + O$ phase, the microemulsion does not go straight into instability.[21] It rather goes through a narrow metastable region. Material exchange between the microemulsion droplets in this unstable phase is still open for debate owing to a subtle balance of droplet interactions, solubility of the oil in the aqueous phase, nature of the surfactant, nature of temperature quench,[22,23,27−30] and so on.

In the present article, we present a systematic temperature quench study of a well-characterized nonionic model microemulsion system consisting of a chlorinated alkane as oil, viz. $C_{12}E_5$/water/1-chlorotetradecane below its emulsification failure boundary (EFB). We have established the detailed phase behavior and material exchange phenomenon of this model microemulsion in our previous reports.[31,32] This microemulsion system is interesting because it has almost the same location of the phase boundaries of the L_1 region as the classical $C_{12}E_5$/water/decane system despite the very different properties of 1-chlorotetradecane (CLTD) compared with decane. Even though CLTD has a longer linear carbon chain with 14 atoms compared with the 10 carbon atoms of decane, it has a much higher solubility in water because it is more polar than decane as a result of the chlorine atom. According to literature values, the solubility of CLTD is about four orders of magnitude larger than that of decane. For CLTD, it is 2.3×10^{-4} g per gram of solution,[33,34] whereas for decane, the value is 2.0×10^{-8} g per gram of solution.[35,36] However, even with the presence of the polar chlorine atom, the surface tension between CLTD and water is very similar to that between decane and water, demonstrating that CLTD is not surface active.[37] Because the properties of the CLTD oil molecules are very different from those of decane, it is interesting to investigate if this has an influence of the phase behavior and separation kinetics; therefore, we investigate in the present article the metastable region below the EFB in the CLTD system in some detail so that the behavior can be compared with that of the decane system.[21]

The emulsification failure of the $C_{12}E_5$/water/CLTD system is initiated by a stepwise temperature quench to the $L_1 + O$ phase, and the corresponding changes in turbidity and light scattering are measured. The changes in turbidity were measured for two different microemulsion droplet volume fractions of 0.02 and 0.08, whereas light scattering was measured only for the droplet volume fraction 0.02. At higher droplet volume fractions, the light scattering measurements could be affected by multiple scattering effects. From these measurements, the presence of metastable and unstable regions in the $L_1 + O$ phase and the kinetic pathway to the new equilibrium in this phase are established.

Experimental Section

Materials. All chemicals were used as received without further purification. High grade pentaethyleneglycol dodecyl ether ($C_{12}E_5$) of purity >98% and CLTD were obtained from Nikko Chemicals and Aldrich, respectively. Milli-Q water was used for the preparation of all samples.

Preparation of Microemulsion. Microemulsion samples containing different droplet volume fractions were prepared by weight at room temperature. The surfactant-to-oil volume fraction ratio (Φ_s/Φ_o), which defines the constraint of the area-to-the-enclosed-volume ratio of the droplets, was fixed at 0.81. For this chosen ratio, nearly spherical microemulsion droplets with maximum curvature toward oil and low polydispersity are obtained.[30,31] Appropriate amounts of $C_{12}E_5$, CLTD, and water were accurately weighed and mixed thoroughly using a high speed vortex mixer for complete homogenization. The samples were heated to 45 °C in an oven and air cooled to room temperature for complete solubilization of the various components of the microemulsion. The weight of each component was then converted to volume using their appropriate density at room temperature ($C_{12}E_5$: 0.978; CLTD: 0.859; water: 0.9980 in units of grams per cubic centimeter). The droplet volume fraction of the microemulsion is defined as

$$\Phi_{\text{droplet}} = \frac{V_s + V_o}{V_s + V_o + V_w} \tag{2}$$

where V_s, V_o, and V_w are the volume of surfactant, oil, and water, respectively.

Preparation of Microemulsion. The exact boundaries of the various phases of the microemulsion as a function of temperature were determined by visual observation, between crossed polarizers, and by turbidity measurements as reported earlier.[31,32,38]

Turbidity Measurements. The turbidity of the microemulsion ($\Phi_{\text{droplet}} = 0.02$ and 0.08) at various temperatures was measured in a Perkin-Elmer Lambda 25 UV−vis spectrophotometer connected to a temperature controller (Perkin-Elmer PTP-1 Peltier system). The temperature of the microemulsion was decreased systematically in steps of 1.0 °C from 20.4 (stable one-phase region) to 15.3 °C (unstable two-phase region), and the change in turbidity at each temperature was measured for ~15 min at a wavelength of 588 nm. The measured turbidity is defined as $\log(I_0/I_t)$, where I_0 and I_t are the incident and transmitted light intensities, respectively. The path-length normalized turbidity (τ) is related to the measured turbidity of the sample, where there is no molecular absorption as[39]

$$I_t = I_0 \exp(-\tau l) \tag{3}$$

$$\tau = \frac{2.303 \times \log(I_0/I_t)}{l} \tag{4}$$

where l is the path-length of light in the cuvette (1.0 cm; Hellma quartz cuvette).

Dynamic Light Scattering Measurements. The diffusion coefficient and the hydrodynamic radius (R_h) of the microemulsion droplets ($\Phi_{\text{droplet}} = 0.02$) were measured by the dynamic light scattering (DLS) technique. Samples for these measure-

ments were prepared under strict dust-free conditions. Samples were transferred to clean and scratch-free cylindrical borosilicate glass cells of inner diameter of 7 mm and centrifuged for 10 min at a speed of 3000 rpm to remove dust particles.

Measurements were performed on a commercially available spectrometer consisting of an ALV/CGS-8F goniometer (ALV GmbH, Germany) equipped with an ALV-6010/EPP multitau digital correlator. The instrument is equipped with an ALV-static and dynamic enhancer with fiber-splitting at 632.8 nm for operation in the pseudo-cross-correlation mode. A helium−neon diode laser (JDS Uniphase) with an output power of 25 mW and operating at a wavelength of 632.8 nm was used as the light source. The incident light was vertically polarized with respect to the scattering plane, and the light intensity was regulated with a software-controlled ALV/8 step beam attenuator.

The normalized intensity−time correlations $g_2(t) - 1$ of the microemulsions at each temperature were measured for 300 s at an angle $\theta = 90°$ The amplitude correlation function $g_1(t) = (g_2(t) - 1)^{1/2}$ was analyzed using the method of cumulants[40] as

$$\ln[g_1(t)] = \ln(A) - \Gamma t + \frac{\mu_2}{2}t^2 - \frac{\mu_3}{6}t^3 + ... \qquad (5)$$

where A is the amplitude, $\Gamma = [\mathrm{d} \ln g_1(t)/\mathrm{d}t]_{t\to 0}$ is the first cumulant, and μ_2 and μ_3 are dimensionless quantities that describe the distribution of relaxation rates.

The mean apparent hydrodynamic radius, R_h, was calculated from the Stokes−Einstein equation as

$$R_h = \frac{k_B T}{6\pi\eta\Gamma} q^2 \qquad (6)$$

where k_B, T, η, and q are the Boltzmann constant, temperature, viscosity of the solvent, and scattering vector, respectively.

The relative polydispersity was calculated from the second moment μ_2 of the second and third order fitting as

$$\frac{\sigma}{R_h} = \frac{\mu_2^{1/2}}{\Gamma} \qquad (7)$$

where σ is the width of the number size distribution and R_h is the average hydrodynamic radius.

Results and Discussion

Metastable and Unstable Region in the L_1 + O Phase. The complete partial phase diagram of the microemulsion $C_{12}E_5$/water/1-CLTD with fixed surfactant-to-oil volume fraction ratio $\Phi_s/\Phi_o = 0.81$ is shown in Figure 1. The details of the occurrence of the various phases have been described in our previous report.[31] The microemulsion droplet phase, L_1, exists in the temperature range 18−25 °C, and the lower phase boundary is not affected by the microemulsion droplet concentration even up to 25 vol %. The lowest temperature (phase boundary) at which all the oil is solubilized in the microemulsion is 18 °C, and this boundary is termed as the EFB. This is indicated as T_{EFB} in Figure 1.

It is well established that in the L_1 phase of the microemulsion (above EFB and up to 25 °C in this case), the microemulsion droplets interact as hard spheres.[30,32,41−43] Below the EFB, the emulsification weakens and breaks down, leading to the formation of a new phase (L_1 + O phase) in which a droplet

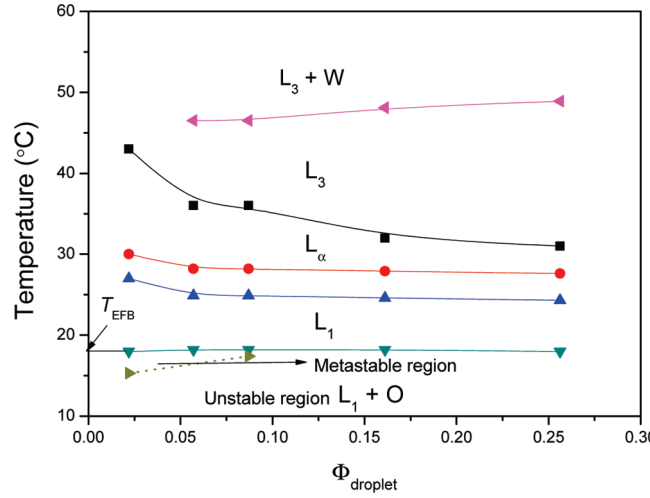

Figure 1. Partial phase diagram of the microemulsion $C_{12}E_5$/water/1-chlorotetradecane at fixed Φ_s/Φ_o of 0.81 for various droplet concentrations, indicating the boundary (dotted line) between metastable and unstable regions within the L_1 + O phase. L_1: microemulsion droplet phase; L_α: bilayers phase; L_3: sponge phase; L_3 + O: sponge phase plus excess water phase.

microemulsion phase is in equilibrium with excess oil as the second phase. The area per surfactant molecule at the interface of the microemulsion droplets is practically constant; therefore, the geometrical constraint that is required to pack a given volume in a given area gives a defined value of the radius of the nonpolar core (R_c) of the microemulsion droplet as

$$R_c = \frac{3\left[\frac{\Phi_s}{\Phi_o} + 0.5\right]V_s}{a_s} \qquad (8)$$

where V_s is the volume of $C_{12}E_5$ = 702 Å^3. The value of 0.5 reflects that approximately half of the total $C_{12}E_5$ molecular volume arises from the volume of the hydrocarbon chain. In eq 8, polydispersity of the droplets is neglected.

At the phase boundary, the optimal radius of the microemulsion droplet matches precisely the spherical radius that is governed by the packing constraints according to eq 8. This is described by Safran[44] as

$$\frac{R}{R_0} = 1 + \frac{\bar{\kappa}}{2\kappa} + \frac{k_B T}{\kappa} f(\Phi) \qquad (9)$$

where κ, $\bar{\kappa}$, and R_0 are the bending rigidity constant, saddle splay constant, and spontaneous radius, respectively. The entropy of mixing the small microemulsion droplets in the continuous medium (water) gives a small contribution, and this is described by the term $(k_B T/\kappa)f(\Phi)$.[45,46]

When the temperature is lowered below the EFB, the spontaneous radius decreases, and to optimize the curvature free energy, the microemulsion droplets respond by expelling the excess oil that it holds. This results in the formation of droplets with new optimal radius ($R_c = R_0$) plus the excess oil in a second phase. For the $C_{12}E_5$/water/decane system, it was shown that the system first passes through a metastable region in which the microemulsion droplets are metastable and then into the unstable region where nucleation of oil-rich droplets occurs and a subsequent growth of the second phase follows.[21]

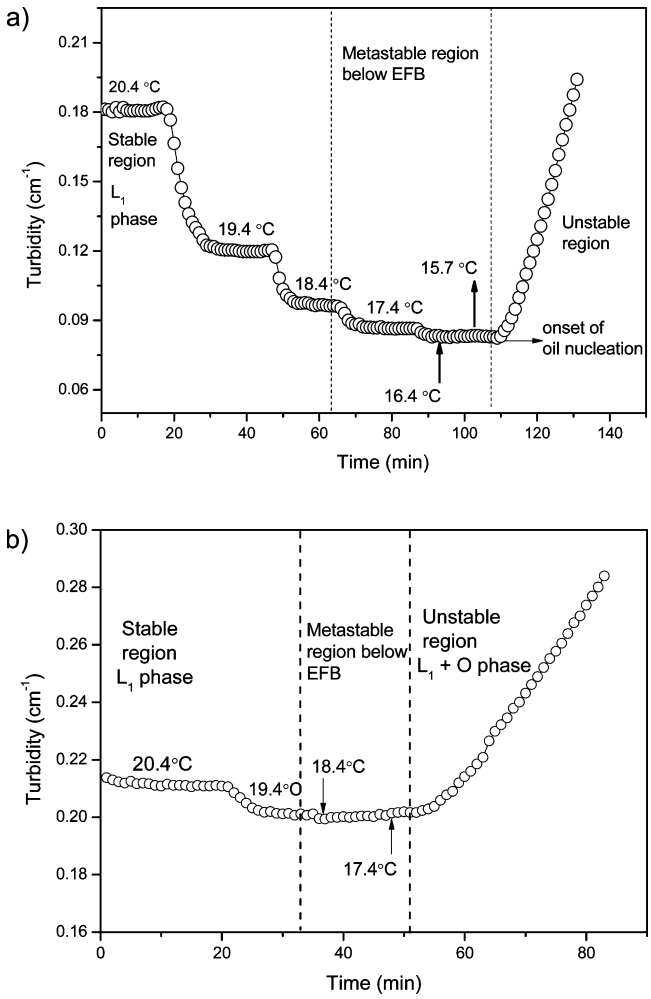

Figure 2. (A) Change in turbidity as a function of time for microemulsion droplets of volume fraction 0.02 upon a systematic temperature quench. (B) Change in turbidity as function of time for microemulsion droplets of volume fraction 0.08 upon a systematic temperature quench.

To determine the metastable and unstable region below the EFB of the CLTD microemulsion, we measured the change in turbidity from slightly above the EFB to the lower temperature region (below the EFB) in steps of 1.0 °C. Figure 2A shows the change in turbidity for a microemulsion droplet of volume fraction 0.02 as a function of time at each quench temperature. At 20.4 °C, the microemulsion is well above the EFB and is thermodynamically stable and optically clear, showing a constant turbidity. When the turbidity remains constant for ∼15 min, we take this as the equilibrium being reached. Upon a quench to 19.4 °C, a large step decrease in turbidity is observed, which comes to a rapid equilibrium indicating fast structural relaxations. The subsequent quenches to 18.4, 17.4, and 16.4 °C also give a stepwise decrease in turbidity but with decreasing magnitude of the steps. The total time that it took for the microemulsion to reach 16.4 from 20.4 °C with the applied stepwise decrease in the temperature was ∼105 min, and remarkably, during this period, no increase in turbidity is observed. This observation of absence of critical fluctuations that one would have in simple binary mixtures, when the spinodal is approached, is attributed to the presence of surfactant film in the microemulsion that gives rise to a free energy barrier.[21,47] This region where there is no increase in turbidity as a result of temperature quench is termed a metastable region.

When the temperature is further lowered to 15.7 °C, no significant decrease in turbidity is observed. The turbidity is stable up to 5 min, beyond which it increases steadily; this defines the onset of the unstable region. The transition temperature from metastable state to the unstable state was determined by zero slope extrapolation of turbidity versus time curve. The transition temperature, $T_{m\rightarrow u}$, thus determined was 15.7 °C, and the final equilibrium in the L_1 + O phase consists of microemulsion droplets and coexisting pure oil. For this droplet volume fraction, the existence of metastable region below the EFB is narrow and only spans 2.7 °C (18.4−15.7 °C). The occurrence of this small metastable region during the systematic temperature quench is attributed to the difficulty of the microemulsion droplets in nucleating larger droplets that grow and form the oil phase. This reflects that there is a free energy barrier as one, for example, has for homogeneous nucleation.[21,47] However, the presence of the surfactant film prevents an increase in concentration fluctuations and hence in turbidity as one has near the spinodal line in simple binary mixtures.[21,47] In contrast, there is actually a decrease in turbidity in the metastable region. This can only be caused by the microemulsion structure becoming more homogeneous. This can be due to either a narrowing of the size distribution or the microemulsion droplets becoming less aspherical as they are known to be due to shape variations.[32,43,48]

For a droplet volume fraction of 0.08 (Figure 2B), an increase in turbidity was noticed when the system was quenched to 17.4 °C, indicating the onset of oil nucleation in the unstable region. The transition temperature $T_{m\rightarrow u}$ for this droplet concentration was 17.8 °C, and the metastable region below the EFB is even narrower, only 0.6 °C (18.4−17.8 °C). This significant decrease in the range of the metastable region as a function of droplet volume fraction is attributed to increasing droplet interactions at high droplet volume fractions. It is interesting to note that for the microemulsion consisting of $C_{12}E_5$/water/*n*-decane,[21] the width of the metastable region was constant (∼ 2.9 °C) even at high droplet concentration, and it was argued that this is a general feature of these microemulsion systems. The main difference between the decane system and the CLTD system is the difference in solubility of the oils in water. The chlorinated oil has a much higher solubility than decane, which means that the concentration of the CLTD in the water phase is much higher. One could speculate that this has an influence on the oil nucleation and the transfer into the larger droplets that grow to form the oil phase.

The boundary between metastable and unstable regions within the L_1 + O phase is indicated by the dotted line in Figure 1. In a homogeneous nucleation situation similar to the present case, some of the microemulsion droplets have to grow in size with time to form the macroscopic oil phase. However, slightly below the EFB and for small temperature quenches, the variation in droplet sizes may not be large enough, and the formation of larger oil-rich droplets correspond to an uphill process because there is initially an unfavorable increase in curvature free energy for the large droplet,[21,27,47] whereas for large temperature quenches and well below the EFB, the gain in curvature free energy for the smallest droplets is so large that it overall gives a downhill process.[21,47] In the unstable region, the larger droplets that will form the oil phase have a narrow size distribution with a form that is nearly time-independent.[30−32] This gives good support for that the growth occurs by the process of Ostwald ripening, which involves diffusion of single oil molecules in the continuous phase. The surfactant film in these large droplets

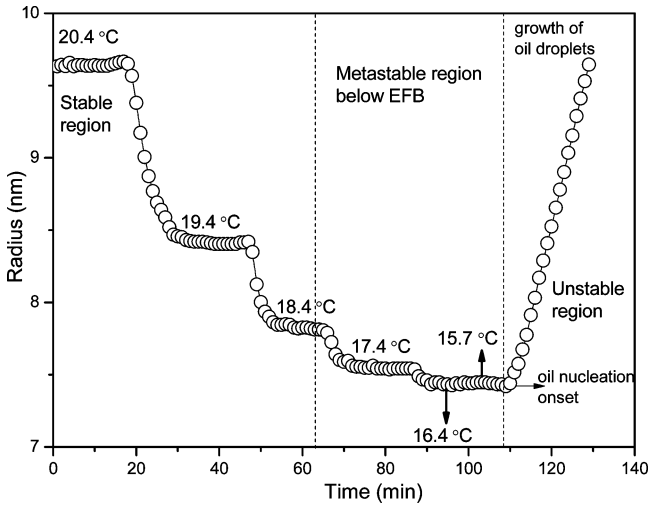

Figure 3. Change in microemulsion droplet radius versus time for a microemulsion droplet volume fraction of 0.02 as a result of systematic temperature quench.

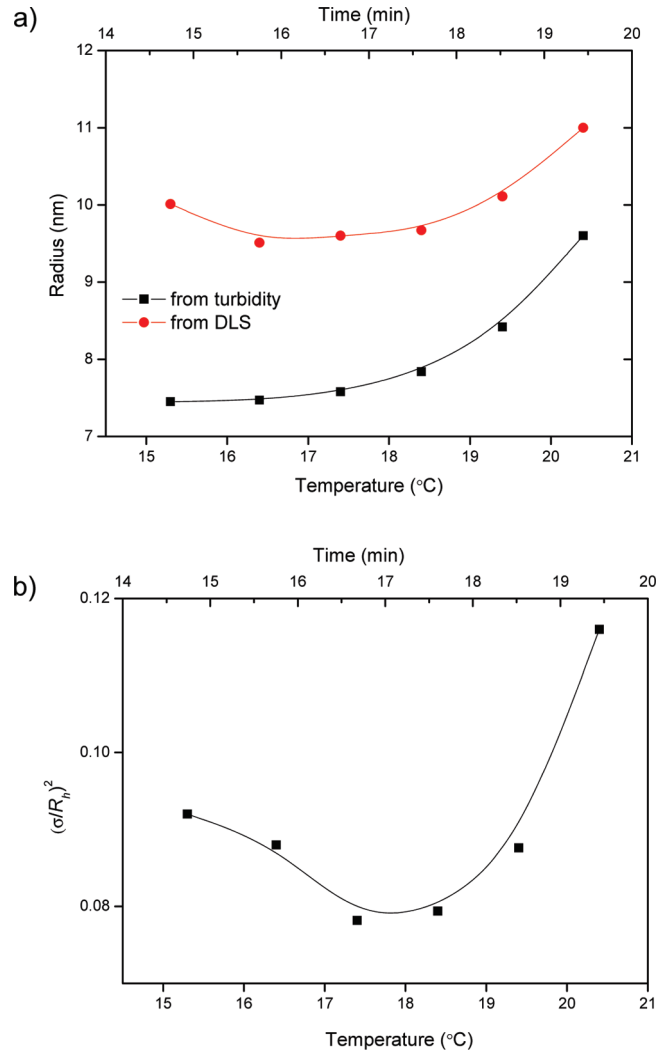

Figure 4. (A) Radius versus quench temperature obtained from turbidity and dynamic light scattering measurements. (B) Relative polydispersity versus quench temperature obtained from dynamic light scattering measurements.

has an unfavorable curvature, and it is the elimination of this surface that drives the growth of the large droplets.

Change of Microemulsion Droplet Size in Metastable and Unstable Regions. The change in turbidity as function of time (for $\Phi_{droplet} = 0.02$) as a result of the systematic temperature quench was converted to a size of the microemulsion droplets using our modified approach as described in detail previously.[32] In this approach, the relatively small polydispersity and small deviations from a spherical shape of the droplets are neglected, and it is assumed that the droplets are monodisperse in size, spherical, and interact via a hard-sphere interaction potential. The structure factor value describing the interaction was in the modeling described by the Carnahan and Starling approximation.[49] In the calculation of the optical constant, the contribution of microemulsion droplets (which dominate the scattering in the L_1 phase and in the metastable region) consisting of surfactant and oil was taken into account. The approach leads to a fifth-order equation for the radius of the droplets, which can be solved iteratively.[50]

A plot of the microemulsion droplet radius derived from the turbidity as a function of time for $\Phi_{droplet} = 0.02$ is shown in Figure 3. The radius of microemulsion droplet at the equilibration temperature of 20.4 °C is 9.2 nm, which reduces to 8.4 nm at 19.4 °C. This radius is stable for the total measurement time of 20 min. Further temperature quenches to 18.4, 17.4, and 16.4 °C leads to very small changes in the size of the microemulsion droplets such as 7.5, 7.45, and 7.4 nm respectively. As mentioned above, this can be due to either a narrowing of the size distribution or the microemulsion droplets becoming less aspherical because they are known to be due to shape variations. This is discussed further below in connection with the DLS results. (See also the Appendix.)

Upon reaching the quench temperature of 15.3 °C, the size of the droplets continues to be stable up to ~10 min, beyond which a linear increase is observed. This increase is due to the expulsion of excess oil by the microemulsion droplets leading to the formation of larger oil-rich droplets that continue to grow. These growing droplets now dominate the scattering process, and the size of the first unstable droplet that can be observed is 7.5 nm, which is in excellent agreement with the size of 7.6 nm determined by the small-angle X-ray scattering method.[32] In the calculation of the size of the droplets in this unstable region, the average contrast factor of the initial microemulsion droplets is used, which holds good just at the onset of instability. In a later stage, the scattering from growing droplets becomes dominated, and the oil contributes more to the actual contrast factor. It is interesting to note that with the temperature variation applied, it takes ~110 min for the microemulsion droplet from the equilibrium size to reach its metastable size (from 9.2 nm at 20.4 °C to 7.4 nm at 15.3 °C), whereas the growth of oil-rich droplets in the unstable region is markedly steep.

The hydrodynamic radius, R_h, and the relative polydispersity, σ/R_h, of microemulsion droplets for $\Phi_{droplet} = 0.02$ were also determined by DLS, and the results along with the radius obtained by turbidity are shown in Figure 4A,B. Although the hydrodynamic radius of the microemulsion droplets is larger than those determined by the turbidity, the behavior of the curve is similar. The hydrodynamic radius decreases from 11 nm above EFB to 9.5 nm at 16.4 °C in the metastable region.

In the unstable region, the hydrodynamic becomes gradually dominated by the oil-rich droplets which are ~10 nm. The relative polydispersity, plotted in Figure 4B, displays initially a pronounced decrease for decreasing temperatures. For the

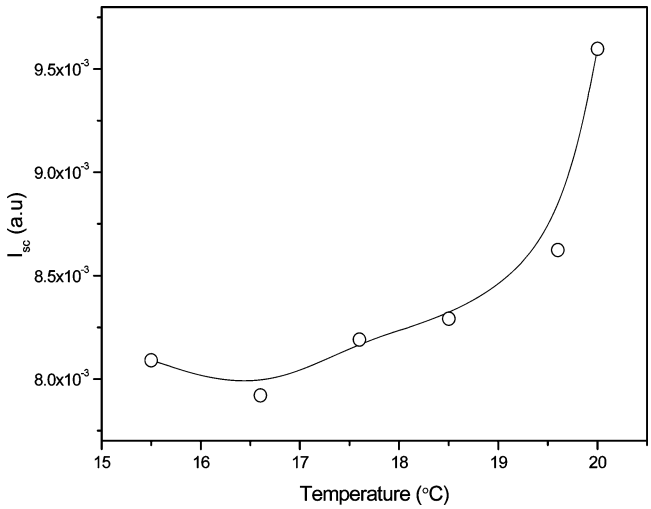

Figure 5. Change in scattered light intensity versus quench temperature for a microemulsion droplet of volume fraction 0.02.

lowest temperature just before the system becomes unstable, it increases slightly. The interpretation of the decrease in R_h and of σ/R_h requires some additional comments. The surfactant is known to have an almost temperature-independent area per headgroup,[21] and because the partial volumes also have a very small temperature dependence, the total surface area of the hydrocarbon part of the droplets (oil and C_{12} chains of surfactant) as well as the volume of the hydrocarbon part can be considered to be conserved. This is used in eq 8 for calculating the radius of the droplets under the assumption that they are spherical and monodisperse. When changes in the hydrodynamic radius are observed experimentally, it therefore means that there are changes in either droplet form or polydispersity. The latter is indeed observed directly in the measurements; however, it is derived under the assumption that the particles are spherical, so it could in fact also be caused by changes in the form of the droplets, that is, that the droplets changes from being on average aspherical to a form closer to spherical. In the Appendix, we calculate the influence on the hydrodynamic radius for variation in eccentricity for monodisperse ellipsoidal droplets and for variation in polydispersity, respectively, both under the constraint of conservation of volume and surface area. The calculations show that the average observed hydrodynamic radius increases both with eccentricity and with polydispersity. Therefore, the observed behavior with a decrease in observed hydrodynamic radius in the metastable region can be due to the droplets becoming more spherical or due to a narrowing of the size distribution or both.

The intensity of scattered light, I_{sc}, as function of temperature is shown in Figure 5. The intensity of light scattered decreases with the systematic temperature quench reflecting the formation of on average smaller droplets in the metastable region in agreement with both turbidity and DLS measurements. At 15.5 °C, it shows an increase indicating the growth of larger oil-rich droplets in the unstable region that dominates the scattering of light. The overall changes in the microstructure of the microemulsion as a result of the systematic stepwise temperature quench are summarized and illustrated in Figure 6.

Conclusions

The response of a dilute oil-in-water microemulsion consisting of $C_{12}E_5$/water/1-chlrotetradecane that was subjected to a systematic stepwise temperature quench has been studied. As for the corresponding decane system,[21] a narrow metastable region exists just below the EFB, and well below the EFB is the unstable region, where there is a large change in preferred droplet surface curvature that facilitates the formation of an excess oil phase in equilibrium with the L_1 droplet phase. In this region, the oil-rich droplets grow over time by the process of Ostwald ripening.[30−32] In the metastable region, turbidity measurements and DLS measurements show that the droplet distribution becomes more homogeneous by a decrease in the eccentricity of the droplets and by a decrease in the polydispersity. The presence of the metastable region is interpreted as the unfavorable change in curvature free energy not being large enough to facilitate the nucleation and growth of oil-rich droplets. For deep temperature quenches well below the EFB, the curvature free energy is favorable for the nucleation and growth of oil-rich droplets in its path toward the new equilibrium. The interpretation of the presence of the metastable and unstable regions is the same as that for the decane system.[21,47] Therefore, despite the very different physical properties of decane and 1- chlorotetradecane, the behavior and the response to the stepwise temperature quench are very similar. However, in contrast with the decane system, the width of the metastable region displays in the chlorotetradecane system a dependence on the droplet concentration.

Acknowledgment. We thank Grethe Vestergaard Jensen, Joakim Balogh, Carsten Svaneborg, Ulf Olsson, and Stefan Egelhaaf for valuable comments and stimulating discussions; Bente Olsen for assistance in the preparation/colloid laboratory; and The Danish Natural Science Research Council (FNU) for financial support.

Appendix

Influence on observed hydrodynamic radius of droplet eccentricity and polydispersity

First, the influence of eccentricity of the droplets is considered. For simplicity, it is assumed that the droplets are monodisperse. We have a volume of

$$V = n\frac{4\pi}{3}R^3\varepsilon \tag{A1}$$

where n is number of droplets, R is their radius, and ε is the eccentricity of the ellipsoid of revolution with semi axis (R, R, εR). V is the total volume of oil and hydrocarbon tails of the surfactant.

We have the following total surface area at the neutral plane

$$S = n\,2\pi R^2\left(1 + \varepsilon\frac{\arcsin(\sqrt{1 - 1/\varepsilon^2})}{\sqrt{1 - 1/\varepsilon^2}}\right) \tag{A2}$$

where we have used the analytical expression for the surface area of a prolate ellipsoid of revolution.[51]

We can isolate $1/n$ in both of these equations and combine these to obtain the following expression for the radius

$$R = \frac{3V}{2S}\left(\frac{1}{\varepsilon} + \frac{\arcsin(\sqrt{1 - 1/\varepsilon^2})}{\sqrt{1 - 1/\varepsilon^2}}\right) \tag{A3}$$

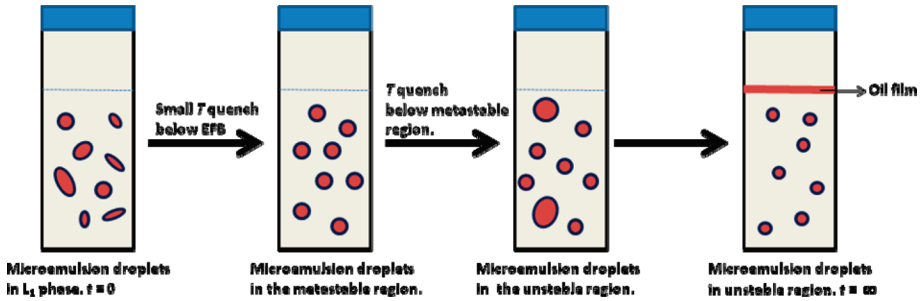

Figure 6. Schematic illustration of microstructural changes of the microemulsion in the metastable and unstable regions of L_1 + O phase as a result of temperature quench.

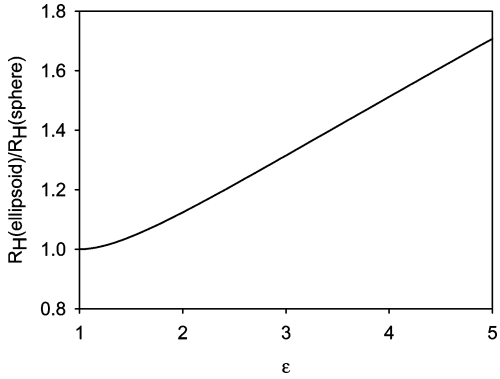

Figure A1. Dependence of the observed hydrodynamic radius on the eccentricity of the droplets.

The equivalent sphere radius is

$$R_S = R\varepsilon^{1/3} = \frac{3V}{2S}\left(\frac{1}{\varepsilon} + \frac{\arcsin(\sqrt{1 - 1/\varepsilon^2})}{\sqrt{1 - 1/\varepsilon^2}}\right)\varepsilon^{1/3} \tag{A4}$$

Using Perrin formula for prolate ellipsoids[52]

$$\frac{R_H}{R_S} = \frac{\sqrt{\varepsilon^2 - 1}}{\varepsilon^{1/3}\ln(\varepsilon + \sqrt{\varepsilon^2 - 1})} \tag{A5}$$

we get

$$R_H = \frac{3V}{2S}\left(\frac{1}{\varepsilon} + \frac{\arcsin(\sqrt{1 - 1/\varepsilon^2})}{\sqrt{1 - 1/\varepsilon^2}}\right)\frac{\sqrt{\varepsilon^2 - 1}}{\ln(\varepsilon + \sqrt{\varepsilon^2 - 1})} \tag{A6}$$

The parameter

$$\frac{S}{3V}R_H = \frac{1}{2}\left(\frac{1}{\varepsilon} + \frac{\arcsin(\sqrt{1 - 1/\varepsilon^2})}{\sqrt{1 - 1/\varepsilon^2}}\right)\frac{\sqrt{\varepsilon^2 - 1}}{\ln(\varepsilon + \sqrt{\varepsilon^2 - 1})} \tag{A7}$$

is the hydrodynamic radius of monodisperse prolate ellipsoidal droplets relative to that of spherical droplets (R_h(ellipsoid)/R_h(sphere)) for a fixed surface-to-volume ratio. The plot in Figure A1 shows that this function is an increasing function of ε; therefore, eccentricity gives a larger observed hydrodynamic radius than that for spherical droplets.

In the following, the effect of polydispersity is considered under the assumption that the droplets are spherical. For the size distribution, a Schulz distribution is used because it allows the calculations to be done analytically.[53,54] The distribution is

$$f(R) = \frac{R^z}{\Gamma(z+1)}\frac{(z+1)^{z+1}}{\bar{R}^{z+1}}\exp(-(z+1)R/\bar{R}) \tag{A8}$$

where $\Gamma(x)$ is the gamma function that for integers is $\Gamma(n+1) = n!$ and fulfils $\Gamma(n+1) = n\,\Gamma(n)$, $\bar{R}$ is the center of mass of the distribution, and $z + 1 = (\sigma/\bar{R})^2$ where σ is the spread of the function.

In general, the moments of this distribution is

$$m(R^k) = \int R^k f(R)\,dR = \bar{R}^k\frac{\Gamma(z+k+1)}{\Gamma(z+1)(z+1)^k} \tag{A9}$$

The total volume within the particles is

$$V = n\frac{4\pi}{3}\bar{R}^3\frac{\Gamma(z+4)}{\Gamma(z+1)(z+1)^3} = n\frac{4\pi}{3}\bar{R}^3\frac{(z+3)(z+2)}{(z+1)^2} \tag{A10}$$

where n is number density of droplets and V is the total volume of oil and hydrocarbon tails of the surfactant.

In addition, we have the following total surface area at the neutral plane

$$S = n4\pi\bar{R}^2\frac{\Gamma(z+3)}{\Gamma(z+1)(z+1)^2} = n4\pi\bar{R}^2\frac{(z+2)}{(z+1)} \tag{A11}$$

We can isolate $1/n$ in eqs A10 and A11 and combine these to obtain the following equation for the average radius

$$\bar{R} = \frac{3V(z+1)}{S\,(z+3)} = \frac{3V}{S}\frac{1}{1 + 2(\sigma/\bar{R})^2} \tag{A12}$$

This actually means that the constraint causes the number-average size to become smaller when there is polydispersity.

The observed hydrodynamic radius is weighted as[55]

$$R_{av} = \frac{m(R^6)}{m(R^5)} = \bar{R}\frac{(z+6)}{(z+1)} \tag{A13}$$

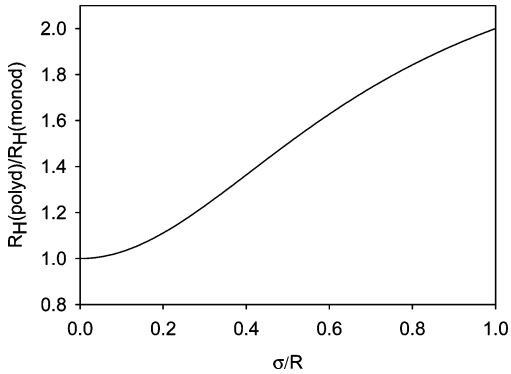

Figure A2. The dependence of the observed hydrodynamic radius on the polydispersity of the droplets.

Using this expression we obtain

$$\frac{S}{3V}R_{av} = \frac{(1 + 5(\sigma/\bar{R})^2)}{(1 + 2(\sigma/\bar{R})^2)} \qquad \text{(A14)}$$

which is an expression for the observed hydrodynamic radius for a polydisperse system relative to that of a monodisperse system (R_h(polyd)/R_h(monod)). This parameter is plotted in Figure A2. The observed hydrodynamic radius increases when the sample is polydisperse when there is a constraint of a fixed total surface and volume. Note that the calculation is not strictly correct because R denotes the radius of the oil + alkyl chain length of the surfactant and not the entire droplet radius. However, the qualitative conclusion is the same even if a shell with constant thickness is added; however, the calculations would be much more involved when including the shell.

References and Notes

(1) Olsson, U.; Wennerström, H. *Adv. Colloid Interface Sci.* **1994**, *49*, 113.
(2) Hellweg, T. *Curr. Opin. Colloid Interface Sci.* **2002**, *7*, 50.
(3) Nagarajan, R.; Ruckenstein, E. *Langmuir* **2000**, *16*, 6400.
(4) Langevin, D. *Annu. Rev. Phys. Chem.* **1992**, *43*, 341.
(5) Solans, C.; Pons, R.; Kuneida, H. *Industrial Applications of Microemulsions*; Kuneida, H., Eds.; Marcel Dekker: New York, 1997.
(6) Deen., G. Roshan; Gan, L. H.; Gan, Y. Y. *Polymer* **2004**, *45*, 5483.
(7) Yaghmur, A.; Aserin, A.; Garti, N. *Colloids Surf., A* **2002**, *209*, 71.
(8) Paul, B. K.; Moulik, S. P. *Curr. Sci.* **2001**, *80*, 990.
(9) Winsor, A. P. *Properties of Amphiphilic Compounds*; Butterworth: London, 1954.
(10) Hamley, I. *Introduction to Soft Matter*; Wiley, 2005.
(11) Burauer, S.; Schert, T.; Sottmann, T.; Strey, R. *Phys. Chem. Chem. Phys.* **1999**, *1*, 4299.
(12) Kuneida, H.; Shinoda, K. *J. Colloid Interface Sci.* **1987**, *118*, 436.
(13) Shinoda, K.; Kuneida, H. *J. Dispersion Sci. Technol.* **1982**, *3*, 233.
(14) Olsson, U.; Nagai, K.; Wennerström, H. *J. Phys. Chem.* **1988**, *92*, 6675.
(15) Strey, R. *Colloid Polym. Sci.* **1994**, *272*, 1005.
(16) Kahlweit, M.; Strey, R.; Firman, P.; Haase, D. *Langmuir* **1985**, *1*, 281.
(17) Kahlweit, M.; Strey, R.; Firman, P. *J. Phys. Chem.* **1986**, *90*, 671.
(18) Kahlweit, M.; Strey, R.; Haase, D.; Kuneida, H.; Schmeling, T.; Faulhaber, B.; Borkovec, M.; Eicke, H. F.; Busse, G.; Eggers, F.; Funck, T.; Richmann, H.; Magid, L.; Söderman, O.; Stilbs, P.; Winkler, J.; Dittrich, A.; Jahn, W. *J. Colloid Interface Sci.* **1987**, *118*, 436.
(19) Sottmann, T.; Strey, R. *J. Chem. Phys.* **1997**, *106*, 8606.
(20) Strey, R. *Colloid Polym. Sci.* **1994**, *272*, 1005.
(21) Morris, J.; Olsson, U.; Wennerström, H. *Langmuir* **1997**, *13*, 606.
(22) Evilevitch, A.; Olsson, U.; Jönsson, B.; Wennerström, H. *Langmuir* **2000**, *16*, 8755.
(23) Taisne, L.; Cabane, B. *Langmuir* **1998**, *14*, 4744.
(24) Ugelstad, J.; Mørk, P. C.; Kaggerud, K. A.; Ellingsen, T.; Berge, A. *Adv. Colloid Interface Sci.* **1980**, *13*, 101.
(25) Pons, R.; Ravey, J. C.; Sauvage, S.; Stébé, M. J.; Erra, P.; Solans, C. *Colloid Surf., A* **1993**, *76*, 171.
(26) Pons, R.; Carrera, I.; Erra, P.; Kuneida, H.; Solans, C. *Colloids Surf., A* **1994**, *91*, 259.
(27) Evilevitch, A. Ph.D. Dissertation, University of Lund, Sweden, 2001.
(28) Egelhaaf, S.; Olsson, U.; Schurtenberger, P.; Morris, J.; Wennerström, H. *Phys. Rev. E* **1999**, *60*, 5681.
(29) Vollmer, D.; Strey, R.; Vollmer, J. *J. Chem. Phys.* **1997**, *107*, 3627.
(30) Roshan Deen, G.; Pedersen, J. S. *Z. Metallkd.* **2006**, *97*, 3.
(31) Roshan Deen, G.; Pedersen, J. S. *Langmuir* **2008**, *24*, 3111.
(32) Roshan Deen, G.; Olivera, C. L. P.; Pedersen, J. S. *J. Phys. Chem. B* **2009**, *113*, 7138.
(33) Staverman, A. J. Ph.D. Dissertation, University of Leiden, 1938.
(34) Horvath, A. L.; Getzena, F. W. *J. Phys. Chem. Ref. Data* **1999**, *28*, 3.
(35) Becke, A.; Ouitzsch, G. *Chem. Technol.* **1977**, *29*, 49.
(36) Haulait-Pirson, M. C.; Hefter, G. T. *Solubility Data Ser.* **1989**, *38*, 295.
(37) Roshan Deen, G.; Jensen, G. V.; Pedersen, J. S., manuscript in preparation.
(38) Sommer, C.; Roshan Deen, G.; Pedersen, J. S.; Strunz, P.; Garamus, V. M. *Langmuir* **2007**, *23*, 6544.
(39) Fletcher, P. D. I.; Suhling, K. *Langmuir* **1998**, *14*, 4065.
(40) Koppel, D. E. *J. Chem. Phys.* **1972**, *57*, 4814.
(41) Olsson, U.; Schurtenberger, P. *Langmuir* **1993**, *9*, 3389.
(42) Fletcher, P. D. I.; Holzwarth, J. F. *J. Phys. Chem.* **1991**, *95*, 2550.
(43) Balogh, J.; Olsson, U.; Pedersen, J. S. *J. Phys. Chem. B* **2007**, *111*, 682.
(44) Safran, S. A. *Statistical Thermodynamics of Surfaces, Interfaces, and Membranes*; Addison-Wesley: Reading, MA, 1994; Vol. 90.
(45) Gradzielski, M.; Langevin, D.; Farago, B. *Phys. Rev. E* **1996**, *53*, 3900.
(46) Kegel, W. K.; Reiss, H. *Phys. Chem. Chem. Phys.* **1996**, *100*, 300.
(47) Wennerström, H.; Morris, J.; Olsson, U. *Langmuir* **1997**, *13*, 6792.
(48) Arleth, L.; Pedersen, J. S. *Phys. Rev. E* **2001**, *63*, 61406.
(49) Carnahan, W. F.; Starling, K. E. *J. Chem. Phys.* **1969**, *51*, 635.
(50) Press, W. H.; Flanney, B. P.; Teukolsky, S. A.; Vetterling, W. T. *Numerical Recipes in Fortran 77*; Cambridge University Press: New York, 1985.
(51) Vass, S.; Pedersen, J. S.; Plestil, J.; Laggner, P.; Retsalvi, E.; Varga, I.; Gilanvi, T. *Langmuir* **2008**, *24*, 408.
(52) Perrin, F. *J. Phys. Radium* **1936**, *7*, 1.
(53) Shev, E. *Phys. Rev. A* **1992**, *45*, 2428.
(54) Capuzzi, G.; Pini, F.; Gambi, C. M. C.; Monduzzi, M.; Baglioni, P. *Langmuir* **1997**, *13*, 6297.
(55) Pusey, P. N. *Neutron, X-rays, and Light: Scattering Methods Applied to Soft Condensed Matter*; Lindner, P., Zemb, Th., Eds.; Elsevier: Amsterdam, 2002.

JP102365J